PMMA removal selectivity to polystyrene using dry etch approach

Aurélien Sarrazin, Nicolas Posseme, Patricia Pimenta-Barros, Sébastien Barnola, Ahmed Gharbi, Maxime Argoud, Raluca Tiron, Christophe Cardinaud

PMMA removal selectivity to polystyrene using dry etch approach

Aurelien Sarrazin[a)]
CEA, LETI, MINATEC Campus, 17 rue des Martyrs, 38054 Grenoble Cedex 9, France and Institut des matériaux Jean Rouxel (IMN), Université de Nantes-CNRS, 2 rue de la Houssinière, 44322 Nantes, France

Nicolas Posseme, Patricia Pimenta-Barros, Sébastien Barnola, Ahmed Gharbi, Maxime Argoud, and Raluca Tiron
CEA, LETI, MINATEC Campus, 17 rue des Martyrs, 38054 Grenoble Cedex 9, France

Christophe Cardinaud
Institut des matériaux Jean Rouxel (IMN), Université de Nantes-CNRS, 2 rue de la Houssinière, 44322 Nantes, France

(Received 17 May 2016; accepted 3 October 2016; published 18 October 2016)

For sub-10 nm technologies, the semiconductor industry is facing the limits of conventional lithography to achieve narrow dimensions. Directed self-assembly (DSA) of block copolymers is one of the most promising solutions to reach sub-10 nm patterns with a high density. One challenge for DSA integration is the removal of poly(methyl methacrylate) (PMMA) selectively to polystyrene (PS). In this paper, the authors propose to study PMMA removal selectively to PS by screening different plasma etch chemistries. The etch mechanisms of the different films have been understood, thanks to x-ray photoelectron spectroscopy analyses performed on blanket wafers. Finally, the best chemistries investigated and being able to remove PMMA selectively to PS have been validated on patterned polystyrene-*block*-poly(methyl methacrylate) copolymer structure. © *2016 American Vacuum Society*. [http://dx.doi.org/10.1116/1.4964881]

I. INTRODUCTION

For sub-10 nm patterns, the semiconductor industry is facing the limits of conventional lithography to achieve narrow dimensions.[1] Based on the technological knowledge (in conventional lithography, deposition and etching processes[2]), multiple patterning is the chosen solution for sub-20 nm patterns.[3] Nevertheless, for the sub-10 nm node, this technique requires a lot of steps to reach these aggressive dimensions and its complexity of integration generates an increase in wafer cost.[4] Today, alternative solutions like extreme ultraviolet lithography or multiple electron beam lithography are under development, but these techniques are not yet mature.[5–8] Therefore, there is a need to develop limitless resolution and low cost techniques such as directed self-assembly (DSA) of block copolymers (BCP).[2,9] Indeed, DSA is one of the promising solutions to reach sub-10 nm patterns with high density. This bottom-up technique will be limited in terms of resolution only imposed by the dimensions of the block-copolymers used.[10]

Different block-copolymers have been studied for sub-10 nm patterning. Polystyrene-*block*-poly(methyl methacrylate) (PS-*b*-PMMA) is the commonly used block-copolymer for DSA applications due to its well-known properties and its easy synthesis.[11,12] Proportions of PS and PMMA on the block-copolymer determine pattern shape.[13] Lamellar or cylindrical PMMA patterns in a PS matrix can be created.[14] According to these properties, line and contact applications could be achieved using DSA.

One of the major challenge for DSA integration concerns PMMA removal selectively to PS. Indeed, it is important to remove the PMMA without altering the PS in order to be able to transfer patterns from the BCP into subjacent layers. This step is very challenging since PS and PMMA present similar bone architecture [see Figs. 1(a) and 1(b)], and thus, achieving a high selectivity between both of them is very challenging. Nowadays, two approaches have been investigated for this PMMA removal: wet or plasma etching. The first approach consists in using a solvent like acetic acid. It has been demonstrated that acetic acid provides an infinite selectivity between these polymers so PMMA can be removed without consuming PS.[15] However, line pattern collapse, due to capillarity forces induced during the solvent development, has been observed on lamellar BCP with an aspect ratio over 1.[15]

Plasma provides better compatibility with narrow lines limiting the risk of pattern collapses for lamellar applications. However, one major drawback of this technique is the difficulty to get high selectivity between PMMA and PS films. Selectivity between PMMA and PS can be expected because the C/O ratio concentration is higher for PS than for PMMA (Ref. 16) and carboxylic compound is not as resistant to the plasma etching as the phenyl group is.[17]

For a while, O_2-based chemistries have been developed to remove PMMA.[18] But the critical dimension control is very challenging since the etching is very reactive[19,20] and presents low selectivity (around 2).[21] Therefore, new chemistries have been proposed in the literature. For example, selectivity has been improved by adding a PS protection step: Chan and Tahara proposed addition of an argon step after Ar-O_2 one.[21] It has been shown that pure argon addition provides a higher PMMA:PS selectivity (around 16:1 on blanket wafers). On lamellar PS-*b*-PMMA films, this argon step is used for protecting PS with the nonvolatile products from PMMA which are deposited on the top of PS patterns during PMMA

a)Electronic mail: aurelien.sarrazin@cea.fr

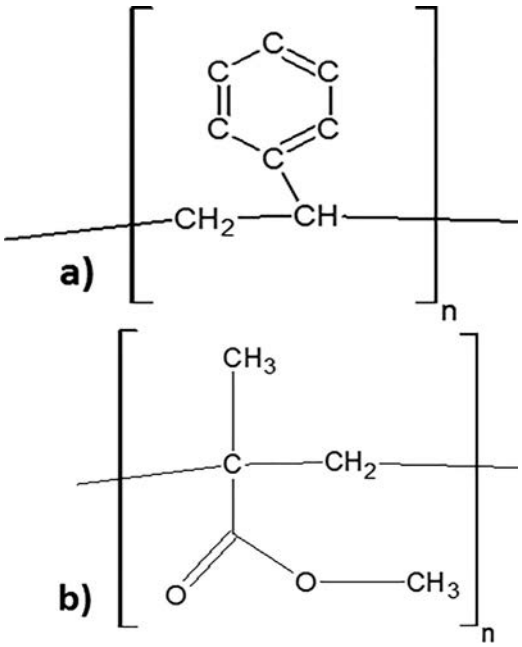

FIG. 1. PS (a) and PMMA (b) semideveloped chemical formulas.

removal.[22] For removing the whole PMMA patterns, Ar-O_2 chemistry is used. This improvement brings a better selectivity PMMA:PS than only Ar-O_2 chemistry and a lower roughness on lamellar copolymers. Nevertheless, the selectivity is lower on PS-*b*-PMMA films than on blanket wafers (only 4:1 on patterns).[22]

Another alternative technique is based on CO-H_2. Omura *et al*. have proposed to use CO chemistry because it provides an infinite selectivity during the first seconds.[23] Then, a saturation phenomenon is observed for PMMA consumption. To overcome this drawback inhibiting PMMA removal, they have decided to add H_2. By controlling ion energy, they have succeeded in achieving a high selectivity on blanket wafers (around 10:1), but the selectivity decreases for its application on PS-*b*-PMMA hole patterns (around 2:1).[23]

In this paper, we propose to determine a chemistry providing a high selectivity between PS and PMMA blanket wafers by plasma etching. This selectivity should allow us to remove PMMA selectively to PS on PS-*b*-PMMA films and to get enough PS material budgets to transfer patterns in the sublayer. To do so, a screening of several gases on PS and PMMA homopolymer wafers has been carried out on 300 mm wafers. Complementary analyses have been performed to understand the mechanisms allowing to get high selectivity between PMMA and PS. Then, best chemistries have been applied on PS-*b*-PMMA film to validate efficiency of the selected chemistry.

II. EXPERIMENT

A. Materials

Polystyrene (PS) and poly(methyl methacrylate) (PMMA) homopolymer solutions, provided by Arkema®, were spin-coated on 300 mm blanket wafers and then annealed on Sokudo Duo™ track to obtain films with a thickness of 50 nm.

Figure 1 shows the formula of PS and PMMA (Ref. 24) [respectively, (a) and (b)].

PS is a polymer composed of an aliphatic carbon and hydrogen backbone chain with a phenyl group (aromatic -C_6H_5) replacing a hydrogen atom every two CH_2 as represented in Fig. 1(a), while PMMA, which is also based on an aliphatic backbone chain, presents methyl (-CH_3) and methacrylate (-$COOCH_3$) groups substituted to the hydrogen atoms every two CH_2 as shown in Fig. 1(b).

PS-*b*-PMMA is a block-copolymer (BCP) composed of PS and PMMA chains. These polymer chains are organized by block, which means that a chain of several monomers from one polymer will be linked to a chain of monomers from the second polymer. This unitary sequence, called period, is repeated several times to obtain the block copolymer [Fig. 2(a)]. The period of the studied polymer, provided by Arkema, is $L_0 = 35$ nm. Then, the BCP is dissolved in propylene glycol monomethyl ether acetate solvent to get a film thickness of 50 nm, and the solution further coated and annealed on Sokudo Duo track.

Our application requires that the patterns organize themselves perpendicularly to the substrate. Therefore, a thin layer should be added below BCP.[25] This layer is a PS-*r*-PMMA, meaning that PS and PMMA monomers are randomly distributed in the copolymer [Fig. 2(b)]. In the

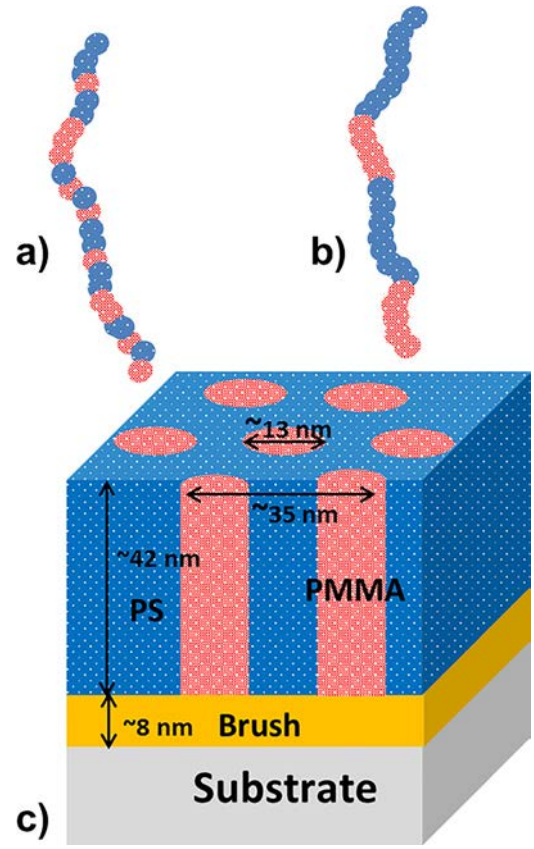

FIG. 2. (Color online) Simplified schemes of PS-*r*-PMMA (a), PS-*b*-PMMA (b), and a cross section of the studied stack composed of a PS-*b*-PMMA film with a cylindrical morphology (c).

TABLE I. Main gas parameters for studied chemistries.

Gas	Pressure (mTorr)	Bias power (2 MHz) (W)	Source power (27 MHz) (W)
CO	120	50	150
Xe	120	50	150
H_2	120	100	500

following, this layer is called brush. The brush and BCP layer thickness are, respectively, around 8 and 42 nm. Copolymers films, obtained with around 33% of PMMA and 67% of PS ($Mn_{PMMA} = 18.5$ kg/mol and $Mn_{PS} = 38.6$ kg/mol) in order to get cylindrical shape, are dedicated to contact patterning applications.

Figure 2 represents simplified schemes of PS-*b*-PMMA, PS-*r*-PMMA, and a cross section of the studied stack composed of a PS-*b*-PMMA film with a cylindrical morphology and a hexagonal meshing (PMMA cylinders in PS matrix).

B. Etching setup

Plasma etching has been carried out on a 300 mm Flex® reactor from LamResearch®. This capacitive coupled plasma reactor has two frequencies (2 and 27 MHz) on the bottom electrode. This bottom electrode has an electrostatic chuck for clamping wafer to etch. An O_2-based waferless auto clean is performed before and after each wafer to assure the same plasma conditions for the different wafers by cleaning the chamber and thus improve the etching process repeatability.

Different gases have been studied for PMMA removal selectively to PS: inert gas (Xe) and reactive gases (CO and H_2). Xenon has been privileged to argon, which has already been widely studied, because it has been proved that it limits the resist striation.[26] Moreover, we have observed a selectivity increase with the ion weight for He, Ar, and Xe (not shown). These gases have been studied in the conditions detailed into Table I. For H_2 plasma, operating conditions are different due to difficulties to plasma breakdown with this low-weight gas.

C. Characterization setup

1. Thickness measurement

Thickness variation established to determine the etch selectivity has been obtained by ellipsometry measurements made before and after plasma etching with an ALERIS HX™ setup from KLA TENCOR™ for an incident angle of 71°. A Cauchy transparent model has been used for thickness measurement from wavelength between 400 and 850 nm for both materials. To take account of the polymer modification induced by plasma, medium index can also be adjusted in the model during the thickness fitting. However, for the etching regime, no index modification has been observed. Pristine PS or PMMA homopolymer thickness is measured around 50 nm.

2. Surface composition

Surface etching mechanism phenomena have been understood, thanks to *ex situ* XPS experiments. These have been carried out on a Thermo Fisher Scientific Theta 300 spectrometer operating with a monochromatic Al Kα x-ray source ($h\nu = 1486.6$ eV). This system allows parallel angle resolved x-ray photoelectron spectroscopy and thus probing different depths of studied material (depth until 10 nm from the surface). The concentrations of C, O atoms are extracted from the C1*s* and O1*s* core-level energy regions, respectively.

Spectral fitting is performed to extract the various peaks contribution in the acquired energy regions. Individual line shapes are decomposed with combination of Lorentzian and Gaussian functions. Each element concentration can be obtained by dividing the calculated peak areas by the corresponding Scofield cross section (O1*s*: 2.93; C1*s*: 1.0). The sum of the concentrations of the different elements present on the analyzed surfaces is equal to 100%.

XPS measurements have been carried out for 10 scans with a dwell time of 500 ms, a pass energy of 50 eV giving a 1 eV spectral resolution. The analyzed surfaces are measured at eight take off angles equally spread between 23.75° and 76.25° relative to the substrate normal. In this paper, we have focused on 23.75° from the normal incidence.

In order to compare the impact of the different plasma chemistries on PS and PMMA, experiments have been carried out at the same time for the different chemistries for each material. Small samples (5×5 cm^2) have been set on the same 300 mm wafer to be characterized without turning the x-ray gun off. Distance between the gun and the different samples is constant.

3. Surface and volume analyses

Scanning electron microscopy (SEM) has been used for morphological observations. A control dimension scanning electron microscopy Hitachi CG4000™ has been used for the determination of shape and dimension patterns. Pictures have been acquired with an accelerating voltage of 500 V and a probe current of 6 pA. Based on SEM images, PMMA cylinder dimensions have been determined by a Matlab™ script with image thresholds.[27] According to this script, the dimensions of 500 cylinders have been determined for each plasma condition. However, the dimensions extracted from this Matlab script are only estimated values as the values are dependent on the threshold parameter. Same threshold parameter has been used for all image treatment performed in this work.

Cross section has been carried out to determine the effectiveness of PMMA removal with Hitachi S5000™. Cross-section samples have been obtained after a gold-palladium metallization of 25 s to reduce charging effect characteristic of the polymer reaction to the electron beam. All the cross sections have been observed at a 350 000× magnification, for an accelerating voltage of 30 keV and a probe current of 10 μA. To determine the PMMA efficiency on cylindrical patterns, 20°-titled images have been taken.

III. RESULTS AND DISCUSSION

A. Polystyrene and PMMA characterization

Figure 3 depicts XPS results obtained on pristine PS and PMMA films.

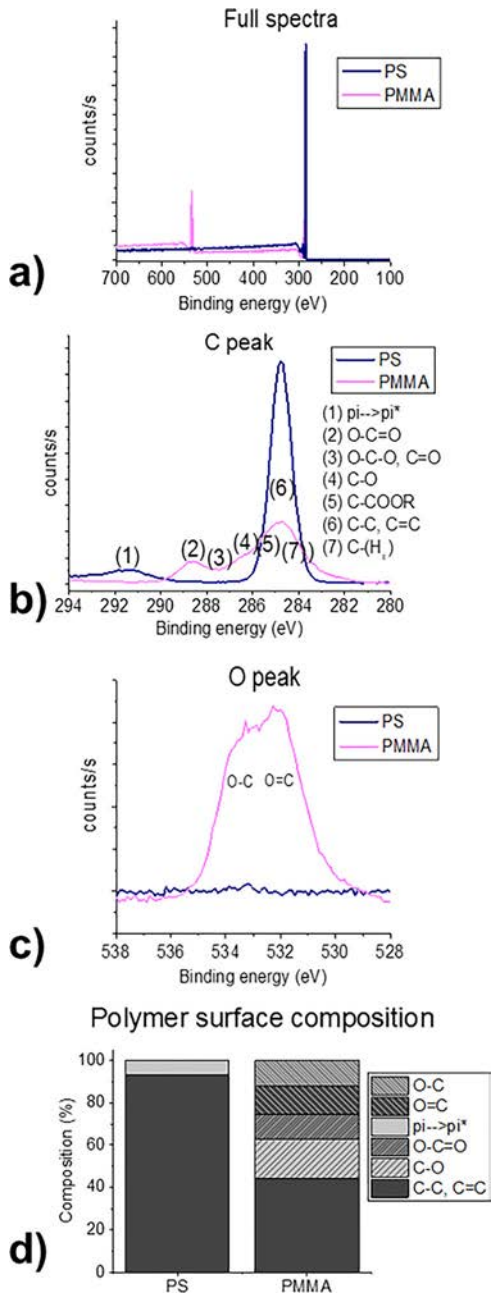

FIG. 3. (Color online) PS and PMMA XPS characterization: pristine PS and PMMA surface XPS full spectra (a), their carbon (b) and oxygen (c) XPS peaks, pristine PS and PMMA atomic composition given by XPS (d).

XPS analyses have been carried out to characterize PS and PMMA composition before and after plasma treatment. First, we have studied pristine PS and PMMA materials. XPS survey reveals that only two peaks are detected on PS and PMMA spectra [Fig. 3(a)]. First peak located at around 285.0 eV represents carbon component, the second one located at around 532.0 eV corresponds to oxygen component.[28] In Fig. 3(b), two peaks have been detected for PS: first peak has been fitted at 285.0 eV, and this peak is assigned to aliphatic carbon and carbon from phenyl cycle. Their characteristic responses are located at 284.7 and 285.0 eV, respectively.[28] Due to the energy pass, we cannot dissociate these contributions. In the following, they will be designated as C–C or C=C peak and not differentiated. A second peak is observed at 292.0 eV, which concerns a shake-up peak characteristic from the aromatic cycle. Concerning PMMA, a first peak is located at 285 eV. This peak can be deconvoluated as the sum of two contributions: carbon from CH_2 and CH_3 bonds at 285.0 eV and C from acrylate compounds at 285.7 eV.[28] However, in the following, C–C or C=C will design the sum of these contributions. A second one located at 286.5 eV assigned to C in the methyl ester (C–O bonds) and a third one located at 288.5 eV corresponding to C in the carboxyl group (O–C=O).[28] These analyses confirm PS and PMMA architectures detailed in Fig. 1.

Oxygen peak has also been analyzed [Fig. 3(c)]: no peak is detected for PS while a large peak for PMMA is observed. This O1*s* peak for PMMA has been analyzed as the combination of O=C (531.5 eV) and O–C (533.0 eV).[28]

According to these analyses, PS and PMMA surface compositions have been determined [Fig. 3(d)]. As expected, PS is fully composed of carbon (hydrogen is not detected by XPS) and PMMA composed by 70% of carbon and 30% by oxygen.

B. PMMA removal selectively to PS on blanket wafers

PMMA removal selectively to PS is a high challenge for DSA integration. In this part, we propose a chemistry screening to provide selectivity between PMMA and PS.

1. Gas screening results

Several gases have been tested on PS and PMMA blanket wafers to determine this selectivity. First, chemically inert gas (Xe) and reactive gases (CO and H_2) have been tested in the plasma etch conditions previously described in Sec. II B.

Figure 4 depicts polystyrene and PMMA consumption as a function of plasma process time for different etch chemistries: xenon, dihydrogen, and carbon monoxide, respectively.

Figure 4(a) shows the PS consumption as a function of the different etch chemistries investigated. The PS consumption increases linearly, from 10 to 95 s, as a function of the process time when using H_2. For instance, the PS consumption increases from 8.6 to 32.8 nm for H_2 plasma process time varying from 10 to 95 s.

In the meantime, PS consumption increases linearly from 3.3 to 9.3 nm between 10 and 65 s followed by a saturation phenomenon when using Xe plasma, characteristics of an etch stop phenomenon. Regarding PMMA, the film is fully removed after 20 s process time when using Xe and H_2 plasmas.

A different behavior is observed for CO chemistry. Indeed, no PS consumption is observed during the first seconds of the plasma while a 3 nm polymer deposition is measured on top of PS after 200 s. In the meantime, 20 nm PMMA is consumed during the only first 10 s. Beyond this time, a film deposition is observed on top of PMMA.

This gas screening study shows that some gases such as Xe or H_2 provide a high PMMA removal rate but a limited PMMA/PS selectivity. Selectivity has been evaluated with the process time for the three gases. After 10 s, the selectivity

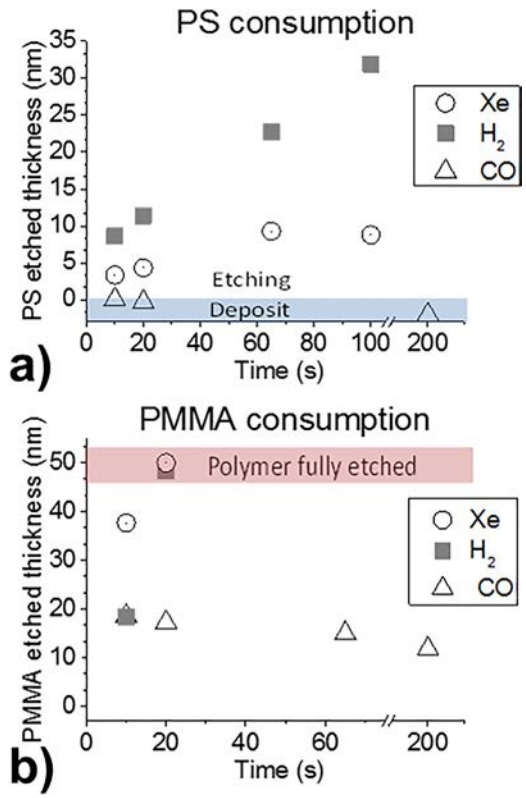

FIG. 4. (Color online) PS consumption (a) and PMMA consumption (b) as a function of the process time for H_2, Xe, and CO plasmas.

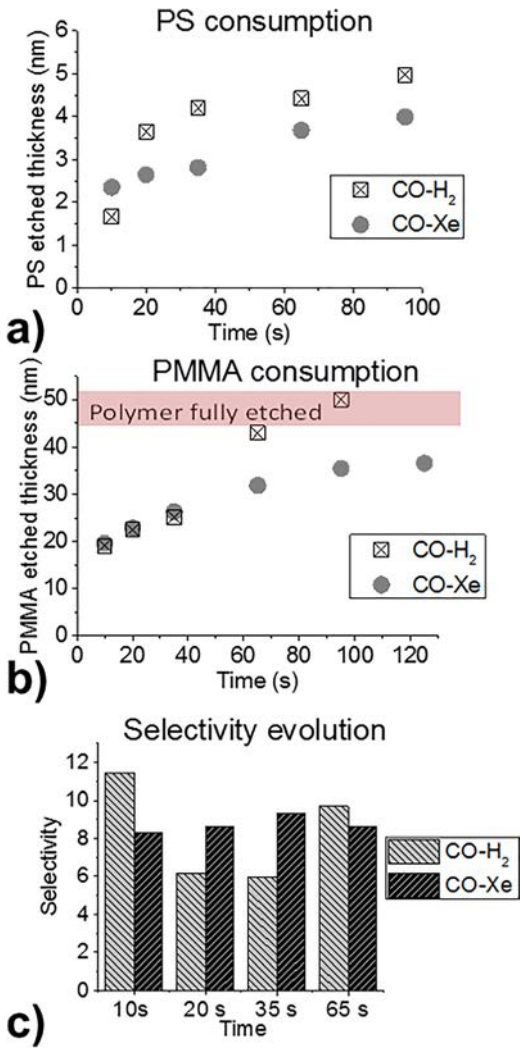

FIG. 5. (Color online) PS consumption (a) and PMMA consumption (b) and selectivity (c) as a function of the process time for CO-H_2 and CO-Xe.

is around 2:1 for H_2 while it above 11:1 for Xe and more than 100:1 for CO. By increasing the process time to 20 s (time necessary to fully remove the whole PMMA film), the selectivity is estimated to be 12:1 and 4:1, respectively, for Xe and H_2. A deposit is created on PS after 20 s, and it gives an infinite PMMA/PS selectivity although PMMA is not etched anymore.

To overcome this issue and to take advantages of the different gases investigated, CO combination with H_2 or Xe has been investigated in order to get a high selectivity without PMMA saturation phenomenon.

2. Gas combinations

In this part, we have investigated CO-H_2 and CO-Xe gas mixtures. Plasma operating conditions are similar to Xe and CO plasma processes described in Table I. The gas ratio has been set at 1:1 with 250 sccm gas, and this ratio has been evaluated as the most promising one.

PS and PMMA consumptions as a function of the different gas mixtures are presented in Fig. 5.

After 20 s plasma processing, PS consumption is estimated to be 3 and 4 nm for CO-Xe and CO-H_2 gas chemistry, respectively. For PMMA consumption, using CO-H_2, a linear consumption is observed for an etching time between 10 and 100 s, with an etch rate estimated to 15 nm/min. Regarding the use of CO-Xe chemistry, two phases can be observed in Fig. 5(b). During the first 35 s of plasma, the etch rate is estimated to 15 nm/min. Beyond this time, PMMA removal rate is slowing down. In our experimental conditions, for 65 s, the PMMA/PS selectivity is about 10:1 for CO-H_2.

To summarize this blanket film study, Xe, CO-Xe, and CO-H_2 (1–1) provide an interesting process window to remove the PMMA selectively to the PS. These experimental results will be further tested and discussed (Sec. III D) in the case of contact patterned structures where 50 nm PMMA domains has to be removed selectively to PS.

C. Etch mechanism understanding

In this part, PS/PMMA etch mechanisms induced by Xe, H_2, CO, CO-Xe, and CO-H_2 plasmas are discussed, thanks to XPS analyses.

1. CO plasma impact on PS and PMMA surface modification

XPS experiments have been carried out studying PS surface for different CO process times (Fig. 6). Spectra have been obtained at 23.75° from the normal incidence.

The C1*s* XPS spectra of PS before and after CO plasma exposure are plotted in Fig. 6(a). The C1*s* spectrum of

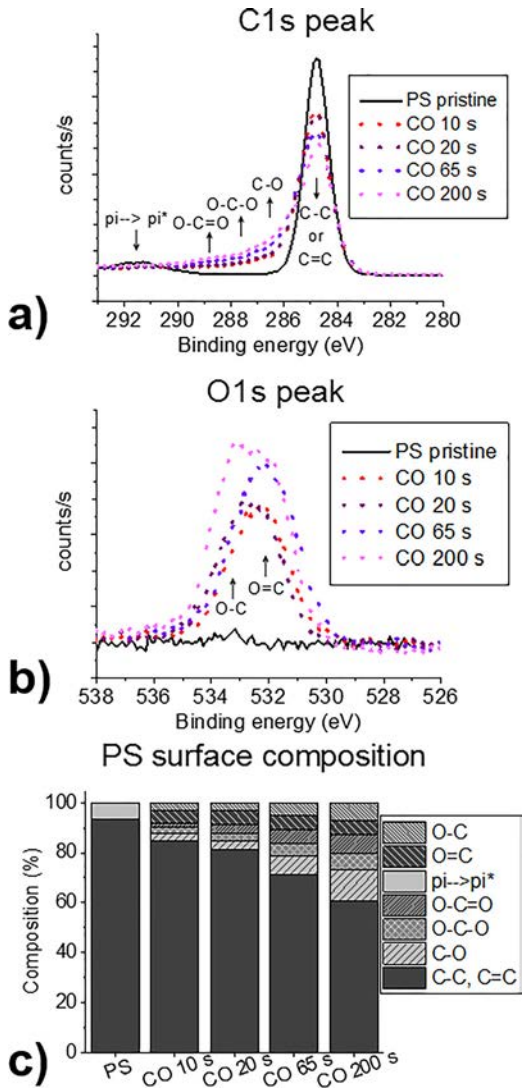

FIG. 6. (Color online) XPS analysis of PS etched in CO plasma carbon peak (a), oxygen peak (b), and surface film composition (c).

pristine PS (black straight line) exhibits one peak at 285.0 eV assigned to C–C or C=C bonds and a second at 292.0 eV assigned to shake up $\pi \rightarrow \pi^*$ component. After few seconds of CO plasma treatment, new peaks located at 286.5, 287.5, and 288.5 eV are observed. They are assigned to C–O, O–C–O (or C=O), and O–C=O bonds,[28] respectively. C–O, O–C–O (C=O), and O–C=O peaks intensity is increasing as a function of the process time. Concerning shake-up $\pi \rightarrow \pi^*$ component, it has disappeared, proving that original PS configuration has been modified.

These bonds are correlated with O1*s* peak deconvolution. The O1*s* peak is a combination of O=C peak (at 531.5 eV) and O–C (at 533.0 eV). The O1*s* contribution is increasing as a function of CO process time, as summarized in Fig. 6(c).

The CO influence has also been studied by XPS on the PMMA blanket (Fig. 7).

The C1s XPS spectra of PMMA before and after CO plasma exposure are plotted in Fig. 7(a). The C1*s* spectrum of pristine PMMA (black straight line) exhibits three peaks: at 285.0 eV for C–C and C=C bonds, at 286.5 eV for C–O bonds, and at 288.5 eV for O–C=O bonds.[28] First seconds of CO plasma seems to break O–C=O bonds, replaced by C–C and C–O and a new contribution O–C–O (C=O). O1*s* peak intensity is decreasing with the CO process time [Fig. 7(b)]. In Fig. 7(c), we can determine two regimes: a first one from 0 to 65 s characterized by an oxygen depletion and a second one from 65 to 200 s with an increase in oxygen content.

Based on the literature[23] and by combining these XPS results with the ellipsometry measurements, we can propose an understanding of the PMMA and PS reaction to CO gas (Fig. 8).

a. 0–65 s. During the first seconds, PMMA is etched by CO gas while PS is not etched (cf. Fig. 4). XPS characterization shows a decrease in the surface density of O–C=O and C–O groups for PMMA. This is consistent with the chemical attack of the material by the plasma species. But it is impossible to determine whether it corresponds to the abstraction of the acrylate group or the individual breaking of the O–C=O and C–O bonds. PMMA etching is thus guided by an overall oxygen depletion. In the meantime, a carbon-oxide based film

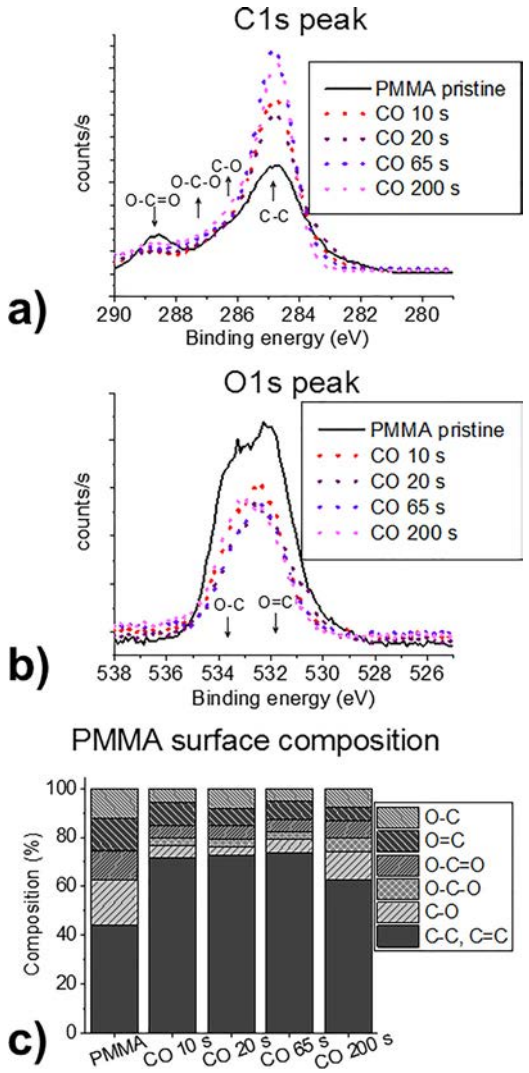

FIG. 7. (Color online) XPS analysis of PMMA etched in CO plasma carbon peak (a), oxygen peak (b), and surface film composition (c).

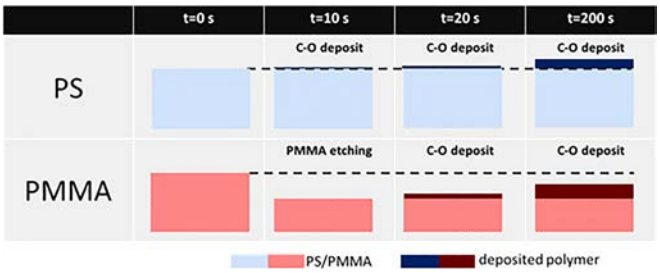

FIG. 8. (Color online) Effects of CO chemistry on PS and PMMA layers.

is deposited on PS. To conclude, the presence of oxygen in the PMMA material allows polymer etching while its absence in PS implies a deposit on this polymer.

b. 65–200 s. Then, at 65 s, we can see that an etching saturation phenomenon is observed for PMMA (Fig. 4). This observation confirms conclusions about CO gas from Omura *et al.*[23] This saturation is characterized by XPS because the initial O–C=O bonds from PMMA pristine material have been substituted to C–O and O–C–O (C=O) bonds after 200 s CO process. This is confirmed by the C–O contribution increase with the process time between 65 and 200 s. By combining ellipsometry and XPS experiments, we can affirm that a C–O deposit is formed on PMMA and is increasing with the CO process time. In the meantime, C–O contribution is increasing on PS as well. We remind that PS is an oxygen free polymer, so the high amount of carbon-oxide bonds revealed by XPS at the top of this polymer proves the deposit observed by ellipsometry. By increasing the plasma time, the deposit on both polymers becomes thicker, as confirmed by the increase of the C–O (O–C–O or C=O) contribution (XPS).

XPS experiments confirm the ellipsometry results about the effect of CO on PS and PMMA: a deposit is observed on PS from the first seconds of CO process and a similar deposit appeared after few seconds on PMMA.

In the next section, the impact of xenon and dihydrogen plasmas on polymer etching is studied.

2. Effect of Xe and H_2 plasmas on the polymer surface

First, the impact of xenon on polystyrene has been evaluated by XPS (Fig. 9).

Figure 9 shows the xenon etching influence on the PS surface. First, we can see that this plasma etching implies a decrease in the density for the C–C and C=C bonds and shake-up component disappearance after xenon plasma treatment [Fig. 9(a)]. In the meantime, C–O, O–C–O (C=O), and O–C=O bonds, which were initially absent, appear and increase in density. This is confirmed by analyzing the *O*1*s* signal: there is an increase in the oxide contribution at the surface after plasma treatment [Fig. 9(b)]. On the other hand, *in situ* experiments (not shown here) have been carried out, showing that no oxygen is detected without air exposure. The observed carbon-oxide bonds are detected because of the *ex situ* experiments. However, another phenomenon has been observed with xenon plasma on PS C1*s* peak: a small peak

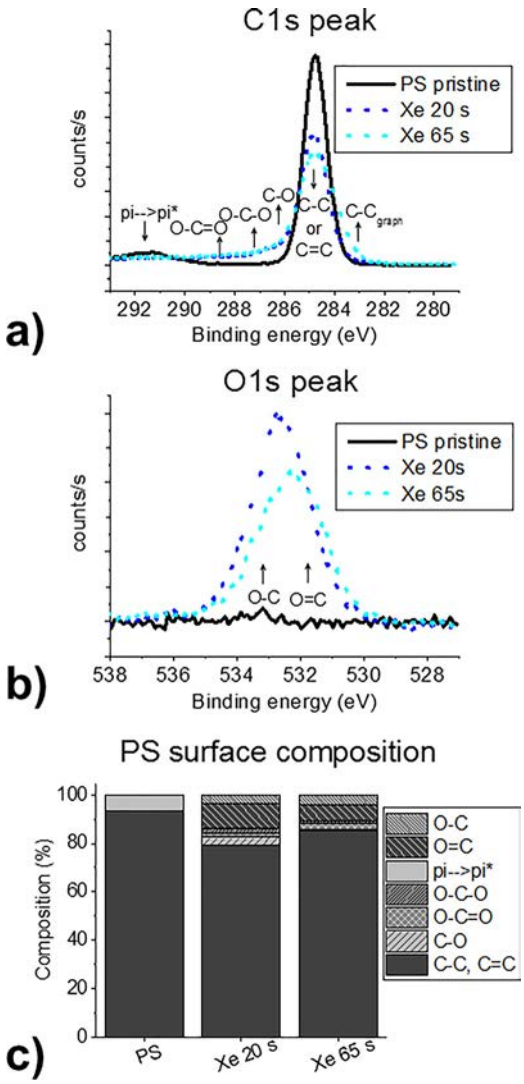

FIG. 9. (Color online) XPS analysis of PS etched in Xe plasma carbon peak (a), oxygen peak (b), and surface film composition (c).

seems to increase with the process time at around 284 eV. This contribution has been explained by Pargon *et al.*[29] to be proof of graphitization of carbon-based material caused by inert gas ion bombardment. It can be deduced that the observed low consumption of PS by xenon chemistry is due to PS reticulation caused by the ion bombardment. This is confirmed by PS consumption after 65 s: etch stop phenomenon is implied by reticulation, as shown in Fig. 4. To conclude, PS is etched by xenon plasma during the first seconds, then it implies a PS reticulation inhibiting its consumption.

The impact of hydrogen on polystyrene has also been evaluated by XPS (Fig. 10).

Similar conclusions to xenon treatment can be proposed with dihydrogen one: a carbon-carbon bond decrease replaced by carbon-oxygen bonds [Figs. 10(a) and 10(b)]. However, it is attributed to *ex situ* experiments, so they are not induced by the plasma. We can observe that H_2 provides a linear etch of PS because the surface composition is similar after 20 and 65 s [Fig. 10(c)]. However, a significant difference with xenon can be detected: no peak has been detected

at 284 eV. It proves different etch mechanisms between Xe and H_2 chemistries.

The same study has also been performed on PMMA films for xenon and dihydrogen at 10 s. Results from these two chemistries have been plotted on the same graph (Fig. 11).

In Fig. 11, xenon and dihydrogen plasma impacts on PMMA layer have been evaluated at 10 s, PMMA thickness is equal to 15 nm for Xe treatment and 30 nm for H_2 (a longer process time cannot be considered due to high etch rate on this material for these gases). Concerning evolution of PMMA surface film for carbon bonds [Fig. 11(a)], we can see that plasma for both gases involves a decrease in the number of C–O and O–C=O groups characteristic from the pristine material. This phenomenon is confirmed by the O1*s* peak study on which we can detect the same intensity decrease [Fig. 11(b)]. In the meantime, C–C bond peak is increasing. These observations are confirmed by Fig. 11(c).

While a similar behavior has been determined for xenon and dihydrogen on PMMA, differences have been observed on PS. Consequently, each plasma follows a different etching mechanism.

First, H_2 mechanisms have been proposed (Fig. 12). We remind that PS and PMMA are etched by H_2 plasma without any saturation phenomenon (cf. Fig. 4).

With dihydrogen chemistry, XPS studies have confirmed ellipsometry results proving PS and PMMA etching. For PS, film composition characterized by XPS is similar between 20 and 65 s, and we have observed apparition of carbon-oxide bonds after the plasma treatment. However, this oxygen contribution does not exist for *in situ* experiments showing that they are not induced by the chemistry. Concerning PMMA, we are in an etching regime confirmed by the full PMMA removal in 20 s with xenon or dihydrogen process time. This etching regime is obtained by depletion of oxygen in the PMMA proved by XPS characterization. This is due to weakness of C–O and O–C=O bonds to the plasma compared to C–C or C=C ones. To summarize, combining ellipsometry and XPS results, we have proved that PS and PMMA are etched by dihydrogen without material modification and without etch stop phenomenon.

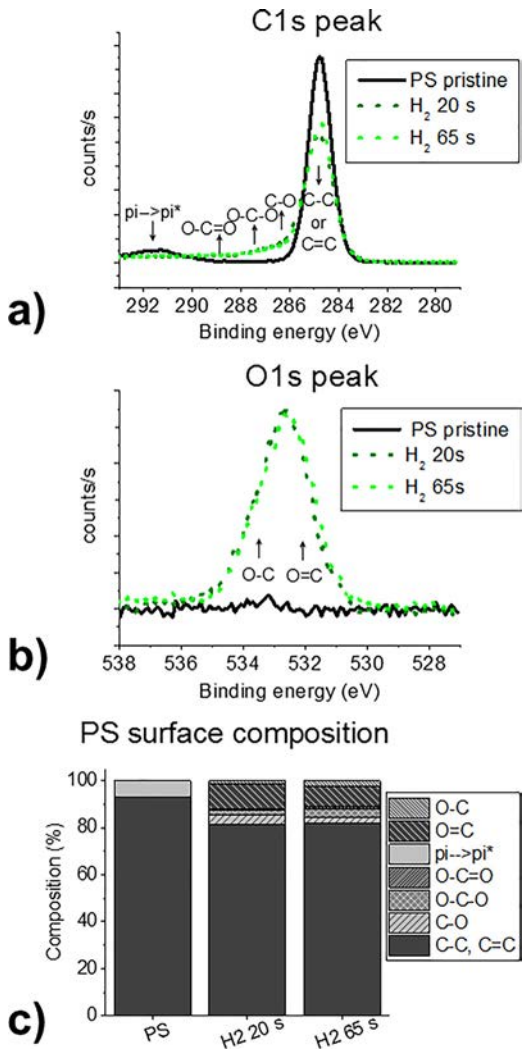

FIG. 10. (Color online) XPS analysis of PS etched in H_2 plasma carbon peak (a), oxygen peak (b), and surface film composition (c).

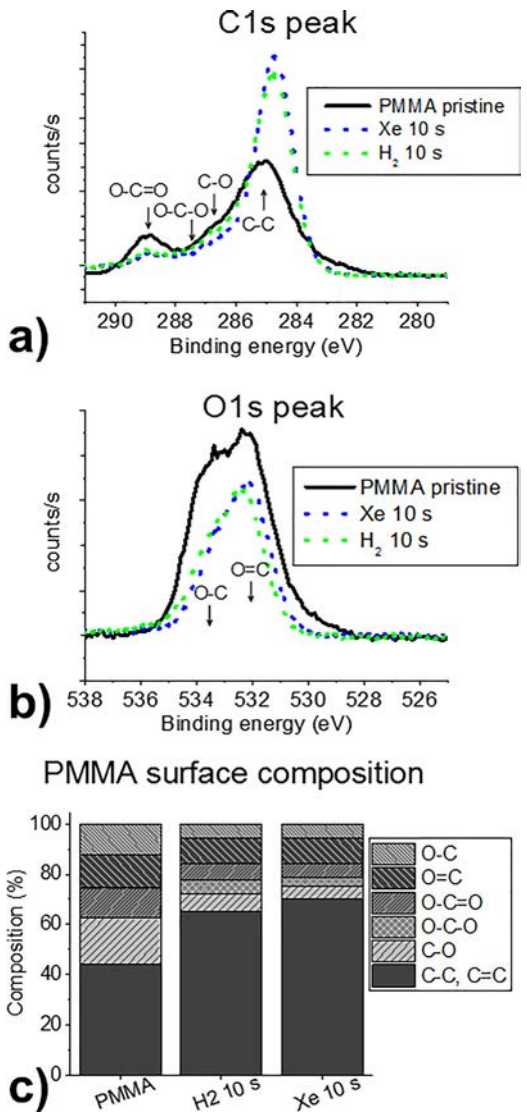

FIG. 11. (Color online) XPS analysis of PMMA etched in Xe and H_2 plasmas carbon peak (a), oxygen peak (b), and surface film composition (c).

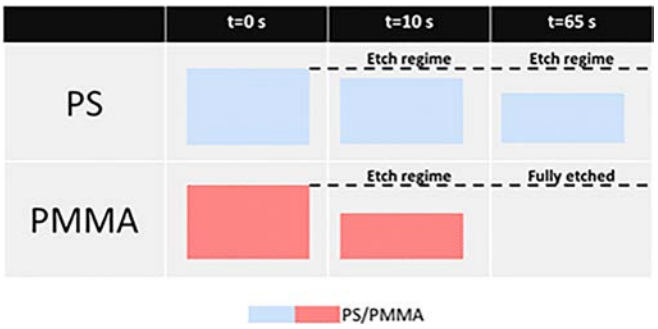

FIG. 12. (Color online) Effects of H_2 chemistries on PS and PMMA layers.

In Fig. 13, the impact of xenon has been studied.

a. 0–20 s. Similar phenomena of H_2 can be proposed for Xe: PMMA and PS are etched during the first seconds. The high PMMA consumption is confirmed by XPS analyses proving similar composition for both gases during the first process seconds. In the meantime, PS is also etched with xenon gas.

b. 20–100 s. A difference between H_2 and Xe plasmas appeared after 20 s with a C-C graphite-like peak present on the *C*1*s* spectra for Xe and not for H_2. This phenomenon observation allows us to prove that xenon ion bombardment will have an effect on PS material. It can be deduced that the observed low consumption of PS by xenon chemistry (cf. Fig. 4) is due to PS reticulation caused by the ion bombardment. This is confirmed by PS consumption after 65 s: an etch stop phenomenon is implied by reticulation. High PMMA/PS selectivity by xenon chemistry has been explained by the PS modification by the xenon while PMMA is etched by oxygen depletion. This advantageous property caused by inert gas has already been used by Omura *et al.*[23] (with argon) for improving selectivity between PS and PMMA with Ar-O_2 chemistry. Oxygen observation in the PS film after xenon treatment is not detectable for *in situ* experiments.

The better PMMA/PS selectivty achieved by Xe compared to H_2 chemistry has been explained by the PS reticulation caused by xenon ion bombardement. We have also confirmed that carbon-carbon bonds (from PS) are more resistant to plasma compared to carbon-oxide ones from PMMA. Finally, we have understood PS deposition and

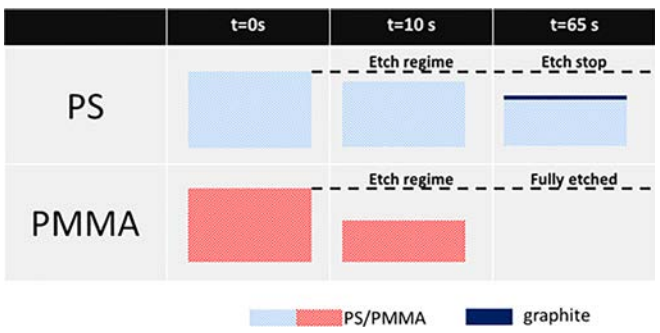

FIG. 13. (Color online) Effects of Xe chemistries on PS and PMMA layers.

PMMA etching stop regime caused by CO gas. By comparing, at 65 s, oxygen amount of PS and PMMA surface composition when using CO, Xe, and H_2 chemistries, we can affirm that a real CO-like deposit is induced by CO gas.

In the following section, Xe and H_2 have been studied combined with CO on PS and PMMA films for understanding surface phenomena implied by these combined chemistries.

3. PS and PMMA surface analyses for CO-Xe and CO-H_2 gas combinations

CO-Xe (1:1) and CO-H_2 (1–1) have been studied on PS films for 20 and 65 s process time.

First, the effects of these chemistries have been evaluated on PS (Fig. 14).

Curves plotted in Figs. 14(a) and 14(b) show apparition of C–O, O–C–O (C=O), and O–C=O contributions. This oxygen contribution is estimated to be 20% [Fig. 14(c)] and it is attributed to *ex situ* experiments. Similar PS surface composition is observed for 20 and 65 s process time indicating that we are in a etch steady state regime.

The same study has been carried out on PMMA (Fig. 15).

Carbon-oxide bonds from PMMA have been favorably deteriorated and substituted by C–C ones [Fig. 15(a)]. Oxygen depletion of PMMA surface has also been highlighted by oxygen decrease at 533.0 eV [Fig. 15(b)]. Finally, these results are confirmed by Fig. 15(c) that depicts the PMMA surface composition before and after the plasma treatments. In this figure, we can detect no significant concentration evolution between 20 and 65 s for CO-H_2. In the meantime, an increase in carbon-carbon bonds instead of carbon-oxygen ones has been observed for CO-Xe.

Based on these XPS results, we have proposed mechanisms involved with these polymers for CO-H_2 and for CO-Xe chemistries.

In Fig. 16, phenomena schematized are those obtained with the CO-H_2 (1:1) chemistry, the best ratio previously determined. We remind that this chemistry allows a full PMMA removal with a 10:1 selectivity to PS (cf. Fig. 5).

With the CO-H_2 chemistry, there is no saturation phenomenon for the PMMA and PS etching, because H_2 plasma chemistry is consuming the carbon-oxide layer formed by CO at the top of the polymer. This is confirmed by the XPS experiments because there is no increase in C–O bonds. By comparing these phenomena with the CO ones, we can prove the interest of gas combination inhibiting the etch stop. By adding H_2, we are succeeding to have an efficient PMMA removal because we have etched almost the whole PMMA film in 65 s (and it is fully etched before 95 s). The high PMMA:PS selectivity (10:1) can be explained by the lower oxygen composition in the PS film compared to the PMMA one.

Even though polymer consumption similarities can be observed for CO-H_2 and CO-Xe, the induced etching phenomena will be different. The proposed etching phenomena for CO-Xe (1–1) are represented in Fig. 17.

CO-Xe chemistry impact on PS is similar to CO-H_2 in terms of polymer consumption and surface composition.

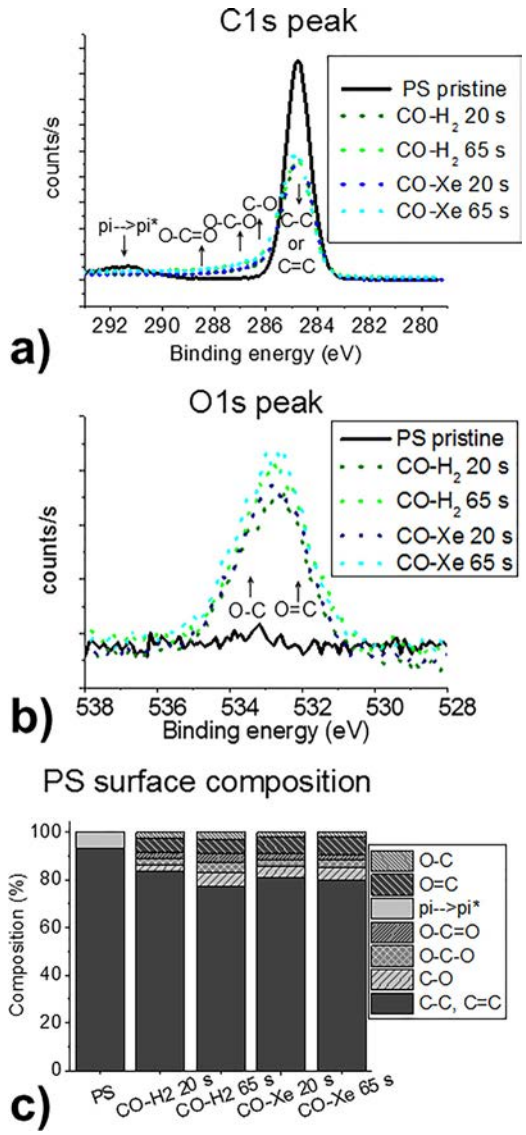

FIG. 14. (Color online) XPS analysis of PS etched in CO-Xe and CO-H_2 plasmas carbon peak (a), oxygen peak (b), and surface film composition (c).

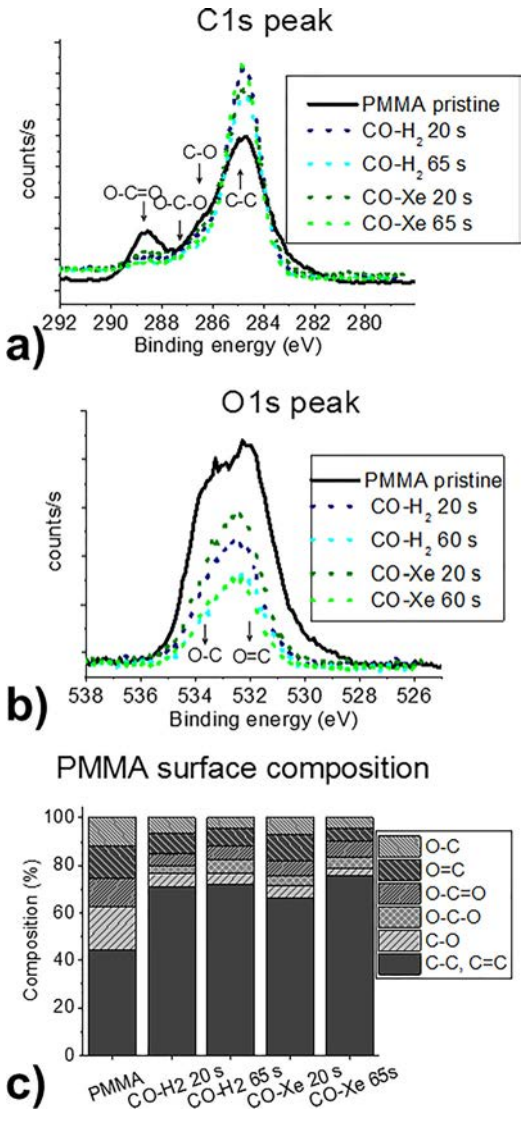

FIG. 15. (Color online) XPS analysis of PMMA etched in CO-Xe and CO-H_2 plasmas carbon peak (a), oxygen peak (b), and surface film composition (c).

While differences had been observed for Xe and H_2 (cf. Figs. 9 and 10), by adding CO to these gases, their behavior seems to be similar for PS. Concerning PMMA, two regimes have been detected (cf. Fig. 5). An etch rate of 15 nm/min is observed during the 65 first seconds and it decreases after. XPS experiments show a slight carbon-carbon bond amount increase between 20 and 65 s. It could be characteristic to saturation phenomenon detected by XPS for xenon chemistry on PS attributed to PS graphitization (cf. Fig. 13).

This discussion about the mechanisms involved in PS and PMMA plasma etching allows us to conclude about the studied plasma chemistries. Concerning CO, it has been shown that during the first seconds PMMA is etched while a deposit is formed on PS. After a few seconds, the same carbon-oxide deposit will be formed on PMMA as well. This deposit will grow up with the process time on both polymers. For dihydrogen and xenon chemistry, an efficient PMMA etch rate has been observed; however, a limited PMMA/PS selectivity has been obtained due to PS consumption. A difference has been noticed between these two chemistries: a saturation phenomenon is observed on PS for xenon while there is a constant PS etch rate for H_2. Xenon ion bombardment implies a graphitization of PS. To improve the selectivity conserving the full PMMA removal, CO-H_2 and CO-Xe gas

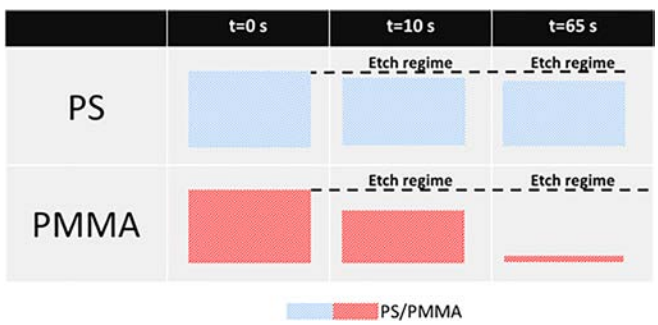

FIG. 16. (Color online) Effects of CO-H_2 chemistries on PS and PMMA layers.

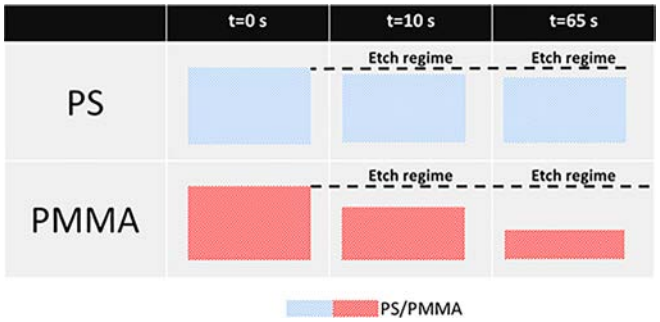

FIG. 17. (Color online) Effects of CO-Xe chemistries on PS and PMMA layers.

combination have been created. CO-H_2 (1:1) has been evaluated as the most interesting chemistry because it allows a full PMMA removal in 95 s with a 10:1 selectivity to PS. In the meantime, a PMMA etch rate decrease phenomenon has been observed for CO-Xe (1:1) confirming that physical gas should not be privileged for polymer etching. Finally, to validate this selectivity study, we have proposed to test the studied chemistries on PS-*b*-PMMA film with a cylindrical morphology.

D. Application to PS-b-PMMA films with cylindrical morphology

The chemistries previously studied have been tested on PS-*b*-PMMA film with a cylindrical morphology.

Figure 18 shows the evolution of PMMA removal selectively to PS on cylindrical patterns for different chemistries (CO, Xe, CO-Xe, and CO-H_2) at 65 s.

The cylinder dimensions experimentally measured after self-assembly are about 11 nm for a 35 nm-pitch [Fig. 18(a)]. First, the top view SEM image of BCP film after CO plasma [Fig. 18(b)] shows a strong reduction of the pattern size (10 nm with nonopened cylinders). This is induced by the important sidewall polymerization. The use of xenon-based chemistries for removing PMMA selectively to PS does not allow good pattern shape conservation [Figs. 18(c) and 18(d)]. Indeed, the polymer is damaged, probably due to bombardment by high mass ions (Xe^+). Xenon-based chemistries cannot be used for cylindrical patterns applications.

Finally, CO-H_2 (1:1) chemistry has been evaluated for the PMMA removal, and this gas combination seems to be the most interesting chemistry in terms of pattern shape conservation. However, a CD bias of around 4 nm is induced by the PMMA removal [Fig. 18(e)].

In Fig. 19, PMMA removal efficiency has been evaluated for different CO-H_2 process times.

All the images have been acquired at similar acquisition conditions. Figure 19(a) allows determining self-assembly pattern thickness: 46.4 nm have been measured in the chosen SEM conditions. After 30 s, 31.6 nm of PMMA have been etched while 6.6 nm of PS have been consumed [Fig. 19(b)]. Thanks to these SEM cross sections, we have determined a PMMA:PS selectivity of around 5:1 on cylindrical patterns. By increasing the process time to 65 s, all the PMMA has been removed, and the brush layer has been etched [Fig. 19(c)] with a 3.5:1 selectivity to PS. Concerning the pattern shape control, the cross section proves that the PMMA removal induced sloped profiles proving the high CD bias observed in Fig. 18(e).

With CO-H_2 mixtures, we have determined a plasma chemistry able to remove PMMA selectively to PS. Morphologic tests on PS-*b*-PMMA films confirm that the CO-H_2 chemistry is a good candidate for this application. This CO-H_2 chemistry has been chosen, thanks to its good PMMA:PS selectivity (10:1), its high PMMA etch rate, and

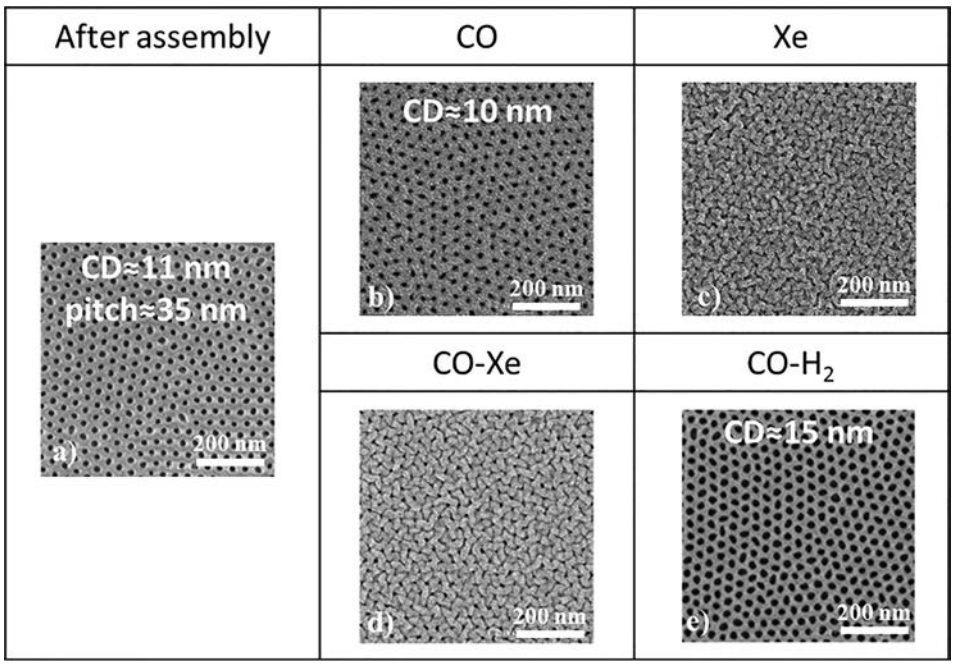

FIG. 18. SEM top view images of cylindrical patterns after self-assembly (a) and after different 65 s-plasma etching using CO (b), Xe (c), CO-Xe (1:1) (d), and CO-H_2 (1:1) (e).

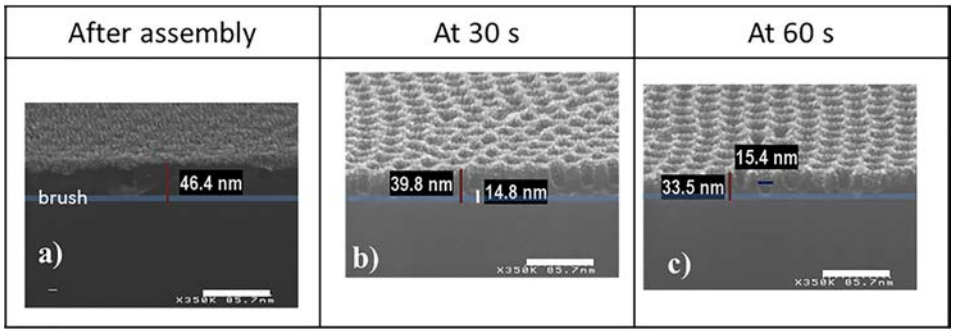

FIG. 19. (Color online) SEM cross section images of cylindrical patterns after self-assembly (a) and CO-H_2 30 s (b) and 60 s (c) process times.

its low PS degradation. Lower selectivity in PS-*b*-PMMA films compared to blanket wafers can be explained by oxygen release from the PMMA to the plasma which plays a role in the PS etching. Selectivity can be improved by an optimization of CO and H_2 ratios. It is possible to reduce the H_2 composition in the fed gas to limit the PS consumption, and the oxygen released in the plasma could be helpful for PMMA removal.

IV. CONCLUSION

A chemistry providing a high PMMA:PS selectivity with an efficient PMMA removal etch rate has been determined on blanket wafers. Among the several tested gases, CO plasma has revealed an interesting behavior leading to a deposit on PS and etching for PMMA, but the saturation phenomenon observed on PMMA after a few seconds of process does not allow using this chemistry for our application. Xenon and dihydrogen plasmas have also been studied. These plasmas allow a full PMMA removal in 20 s, but they consume PS as well. Finally, a trade-off between selectivity and PMMA removal efficiency has been obtained by combining CO with H_2 or Xe.

XPS analyses have been performed to understand mechanisms involved by the different chemistries. Deposits formed on PS and PMMA after few seconds in CO plasmas have been characterized. We have revealed that a CO-like deposit is created. XPS shows that this layer increases with the process time. XPS study has also revealed an important difference between xenon and dihydrogen impact on polymer: a new contribution observed on the carbon C1*s* peak reveals a graphitization of PS when using xenon. This phenomenon explains the lower PS consumption and its etch stop after 65 s. The absence of this phenomenon with dihydrogen confirms the effect of heavy-ion (Xe^+) on PS reticulation. Then, the addition of H_2 or Xe to CO prevents the carbon-oxide deposit on PMMA. A full PMMA removal has been achieved in 95 s for CO-H_2 (1:1) while PMMA consumption is lower for CO-Xe. XPS experiments confirm PMMA etching saturation phenomenon for CO-Xe probably caused by xenon ion bombardment. Finally, ellipsometry results combined with XPS analyses have proved that CO-H_2 chemistry (1–1) allows a full PMMA removal with a 10:1 selectivity to PS.

The developed plasma chemistries have been applied to PS-*b*-PMMA with a cylindrical morphology. We have confirmed the interest of CO-H_2 chemistry for PS-*b*-PMMA film applications.[30] Indeed, it allows a full PMMA removal and a brush etching in a single step. However, a lack of pattern control has been observed during the PMMA removal. Moreover, the low selectivity (5:1) does not assure us a successful pattern transfer to subjacent layers for a microelectronic scheme.

In an upcoming paper, we will propose an optimization of the developed chemistry to overcome these drawbacks. This new chemistry will allow us to compare PMMA removal selectively to PS on cylindrical patterns by plasma etching with the wet approach.[31]

[1]H. J. Levinson, *Principles of Lithography*, 3rd ed. (SPIE, Bellingham, WA, 2010).
[2]S. Barnola *et al.*, Proc. SPIE **9054**, 90540E (2014).
[3]International Technology Roadmap for Semiconductors, 2013.
[4]Y. Chen, Q. Cheng, and W. Kang, Proc. SPIE **8326**, 832620 (2012).
[5]T.-S. Eom *et al.*, Proc. SPIE **8679**, 86791J (2013).
[6]T. S. Kulmala, M. Vockenhuber, E. Buitrago, R. Fallica, and Y. Ekinci, Proc. SPIE **9422**, 942204 (2015).
[7]M. Krysak, M. Leeson, E. Han, J. Blackwell, and S. Harlson, Proc. SPIE **9422**, 942205 (2015).
[8]B. J. Lin, Proc. SPIE **8323**, 832302 (2012).
[9]M. P. Stoykovich and P. F. Nealey, Mater. Today **9**, 20 (2006).
[10]R. R. Dammel, J. Photopolym. Sci. Technol. **24**, 33 (2011).
[11]R. Tiron *et al.*, Proc. SPIE **8323**, 83230O (2012).
[12]X. Chevalier *et al.*, Proc. SPIE **8680**, 868006 (2013).
[13]I. W. Hamley, *Developments in Block Copolymer Science and Technology* (Wiley, Chichester, 2004).
[14]R. A. Segalman, Mater. Sci. Eng. R **48**, 191 (2005).
[15]P. Pimenta Barros *et al.*, Proc. SPIE **9054**, 90540G (2014).
[16]H. Gokan, S. Esho, and Y. Ohnishi, J. Electrochem. Soc. **130**, 143 (1983).
[17]G. S. Oehrlein, R. J. Phaneuf, and D. B. Graves, J. Vac. Sci. Technol., B **29**, 010801 (2011).
[18]C.-C. Liu, P. F. Nealey, A. K. Raub, P. J. Hakeem, S. R. J. Brueck, E. Han, and P. Gopalan, J. Vac. Sci. Technol., B **28**, C6B30 (2010).
[19]R. A. Farrell, N. Petkov, M. T. Shaw, V. Djara, J. D. Holmes, and M. A. Morris, Macromolecules **43**, 8651 (2010).
[20]M. Delalande, G. Cunge, T. Chevolleau, P. Bézard, S. Archambault, O. Joubert, X. Chevalier, and R. Tiron, J. Vac. Sci. Technol., B. **32**, 051806 (2014).
[21]B. T. Chan and S. Tahara, "Etching method using block-copolymers," U.S. patent 0,131,839 (15 May 2013).
[22]B. T. Chan, S. Tahara, D. Parnell, P. A. Rincon Delgadillo, R. Gronheid, J.-F. de Marneffe, K. Xu, E. Nishimura, and W. Boullart, Microelectron. Eng. **123**, 180 (2014).
[23]M. Omura, T. Imamura, H. Yamamoto, I. Sakai, and H. Hayashi, Proc. SPIE **9054**, 905409 (2014).
[24]*Physical Properties of Polymers Handbook*, edited by J. E. Mark, 2nd ed. (Springer, New York, 2006).

[25]P. Mansky, Y. Liu, E. Huang, T. P. Russell, and C. Hawker, Science **275**, 1458 (1997).
[26]N. Y. Babaeva, J. K. Lee, and J. W. Shon, J. Phys. D: Appl. Phys. **38**, 287 (2005).
[27]M. Argoud *et al*., Proc. SPIE **9049**, 904929 (2014).
[28]G. Beamson and D. Briggs, *High Resolution XPS of Organic Polymers: The Scienta ESCA300 Database* (Wiley, Chichester 1992).
[29]E. Pargon, K. Menguelti, M. Martin, A. Bazin, O. Chaix-Pluchery, C. Sourd, S. Derrough, T. Lill, and O. Joubert, J. Appl. Phys. **105**, 94902 (2009).
[30]T. Imamura, H. Yamamoto, M. Omura, I. Sakai, and H. Hayashi, J. Vac. Sci. Technol., B **33**, 061601 (2015).
[31]A. Gharbi, R. Tiron, P. Pimenta Barros, M. Argoud, I. Servin, X. Chevalier, C. Nicolet, and C. Navarro, J. Vac. Sci. Technol., B **33**, 51602 (2015).